Chemical Papers (2022) 76:6017–6031
https://doi.org/10.1007/s11696-022-02317-7

REVIEW

An overview on collision dynamics of deformable particles

Zohre Alinejad[1] · Morteza Bayareh[1] · Behzad Ghasemi[1] · Afshin Ahmadi Nadooshan[1]

Received: 2 May 2022 / Accepted: 31 May 2022 / Published online: 25 June 2022

Abstract
Interaction dynamics of rigid/deformable particles are included in a wide range of industrial and scientific approaches. The description of the binary collision of particles is required to predict the flow of a concentrated emulsion. The present review introduces the numerical approaches employed to simulate the interaction of two particles and evaluates the impact of deformability, configuration, and flow type on collision dynamics. Two closely interacting drops/bubbles can collide in in-line and side-by-side configurations in Newtonian and non-Newtonian surrounding fluids. Based on the previous investigations, the future trends for the binary collision of deformable particles are provided.

Keywords Binary collision · Drop · Bubble · In-line · Side-by-side

Abbreviations

Ar	Archimedes number
Bo	Bond number
Ca	Capillary number
d	Particle diameter, m
Eo	Eötvös number
g	Gravity acceleration, m/s^2
Ga	Galileo number
F	The force due to surface tension, N
F_b	Body force, N
F_{MP}	Added mass force, N
F_D	Drag force, N
F_B	Buoyancy force, N
F_L	Shear-induced lift force, N
K	Solid-fluid viscosity ratio
M	Mobility potential
Mo	Morton number
n	Power-law index
n	Unit vector normal to the drop surface, m
S	Second-order tensor
U	Fluid velocity, m/s
U_p	Particle velocity, m/s
x	Position in an Eulerian coordinate, m
X	Position of the front in Lagrangian coordinate, m

Greek letters

δ^β	Two- or three-dimensional delta function
ϵ	Dissipation rate
η	Viscosity ratio
η_K	Kolmogorov length scale, m
κ	Twice the mean curvature for three-dimensional flows
κ'	Consistency index
λ	Elastic relaxation time, s
λ_1	Relaxation time, s
λ_2	Retardation time, s
μ_o	Zero shear rate
μ_∞	Infinite shear rate
μ_d	Drop dynamic viscosity, Pa.s
μ_f	Fluid dynamic viscosity, Pa.s
ρ_d	Drop density, kg/m^3
ρ_f	Fluid density, kg/m^3
ρ_l	Liquid density, kg/m^3
σ	Surface tension, N/m
φ	Chemical potential
Φ	Volume fraction
Ω	Vorticity tensor
τ	Stress tensor, Pa

Introduction

Interaction between particle/droplet/emulsion in fluid flow is important in many industrial and scientific fields. Multiphase flow presents in nature, including rain droplets, waterfall mists, sediment-laden river flows, and buoyant bubbles in

✉ Morteza Bayareh
m.bayareh@sku.ac.ir

✉ Behzad Ghasemi
ghasemi@sku.ac.ir

[1] Department of Mechanical Engineering, Shahrekord University, Shahrekord 8818634141, Iran

stratified cluster atmospheres (Elghobashi 2019; Zhang et al. 2018) and engineering applications, involving pharmaceuticals, foods, electronics, vitamins, and enzymes (Ding et al. 2019).

Previous works have demonstrated that solid particles have different behavior in fluid flow (Segre and Silberberg 1961; Starkey 1955). For many years, the dynamic and rheology of the deformable object were very challenging. Taylor (1932) presented the deformation of a spherical droplet in Couette flow and developed an analytical relation to predicting the deformation of droplets and emulsions (Taylor 1934). Taylor supposed that deformations are small and inertial effects are negligible. Shapira and Haber (1990) improved Taylor's formula. Afterward, analytical studies presented many results on deformation (Acrivos and Lo 1978; Barthes-Biesel and Acrivos 1973) and breakup (Acrivos 1983; Van Puyvelde et al. 2000) of a drop/bubble in Stokes regime (Friedlander 1961), Couette flow (Busuke and Tatsuo 1969; Chin and Han 1980), and extensional flow (Youngren and Acrivos 1976; Liu et al. 2018a, b, c). Several numerical techniques were used to simulate multiphase flows (Soligo et al. 2020), such as the phase-field method (Soligo et al. 2019; Yue et al. 2006), Lattice Boltzmann method (LBM) (Takada et al. 2003; Ioannou et al. 2016), front tracking (Sun et al. 2019; Bayareh and Mortazavi 2013), etc.

A rigid particle moves toward the center of the channel in simple shear flow and rotates with a constant angular velocity independent of position and initial velocity; however, the equilibrium position of a deformable drop depends on its density ratio, viscosity ratio, deformability, etc. Two rigid particles moving in a shear flow without colliding with each other create a repulsive force due to the existence of the rotational zone created between the two particles. This force is more intense as the two particles get closer to each other. The collision of two particles depends on their initial position and Reynolds number. As the rigidity is reduced and the capillary number decreases, two deformable particles move towards the center of the channel and become closer to each other than the rigid ones. The collision dynamics of two deformable particles depends on the competition between the disjoining pressure and the Laplace pressures. When the disjoining pressure is comparable to the Laplace pressures, the deformable particles will deform.

Various applications of single-phase/multiphase flow laden with rigid/deformable particles have led to publishing many review papers, focusing on the special aspects, such as microfluidic production of multiple emulsions (Vladisavljević et al. 2017), two-phase flows in macro- and micro-devices (Sattari et al. 2020), turbulent flows containing deformable particles (Elghobashi 2019), two-phase bubble columns (Besagni et al. 2018), gas-liquid-liquid multiphase flows (Chen et al. 2019), double emulsions prepared by two-step emulsification (Ding et al. 2019), deformable drop/bubble interactions (Wang et al. 2015), rigid and deformable particles passing through sharp or linearly stratification (Magnaudet and Mercier 2020), and their hydrodynamic collision in non-Newtonian fluids (Zenit and Feng 2018).

The deformation, breakup, and coalescence of deformable particles are due to that the fluid circulates in them internally, leading to their different behavior (Mathai et al. 2020). On the other hand, double emulsions show similar trajectories and different deformation during their interaction in comparison with the deformable drops with a single phase (Liu et al. 2018a, b, c).

In this review paper, the effect of deformability, flow type, and configuration of deformable particles on their collision mechanism is examined and several papers are described. The paper is organized as follows: Sect. 2 introduces non-dimensional parameters used to describe two-phase flows. Governing equations are explained in Sect. 3. In Sect. 4, different configurations of interacting drops/bubbles are described. Section 5 demonstrates the impact of surrounding flow type on collision dynamics and, finally, Sect. 6 provides conclusions and future trends.

Dimensionless parameters

Several dimensionless parameters characterize the interaction of rigid/deformable particles in Newtonian fluids. Table 1 presents dimensionless numbers and their definitions.

Governing equations

Governing equations for Newtonian fluid flow include continuity and Navier–Stokes equations that are described as follows, respectively (Tryggvason et al. 2011):

$$\frac{\partial \rho}{\partial t} + \nabla.(\rho \boldsymbol{u}) = 0 \tag{1}$$

$$\rho\left(\frac{\partial \boldsymbol{u}}{\partial t} + \boldsymbol{u}.\nabla \boldsymbol{u}\right) = -\nabla P + \boldsymbol{F}_b + \nabla.\boldsymbol{\tau} \tag{2}$$

Based on the properties of fluid flow and particles, governing equations of ambient fluid can be simplified and coupled with the equations of particles. Based on the deformability, particles are classified into deformable and rigid particles. Due to the presence of particles in fluid flow and their influences on the hydrodynamics of ambient fluid, the particle-laden flows are assumed to be turbulent. Different numerical approaches are described for rigid and deformable particles.

Table 1 Dimensionless parameters that characterize multiphase flows

Dimensionless parameter	Formulation
Bulk Reynolds number	$Re_b = \frac{\rho_f UL}{\mu_f}$
Particle Reynolds number	$Re_p = \frac{\rho_f U_p d}{\mu_f}$
Archimedes number	$Ar = \frac{\rho_f g d^3 \Delta\rho}{\mu^2}$
Bond number	$Bo = \frac{\rho g d^2}{\sigma}$
Eötvös number	$Eo = \frac{\Delta\rho g d}{\sigma}$
Capillary number	$Ca = \frac{\mu_f U}{\sigma}$
Morton number	$Mo = \frac{\mu_f^4 g \Delta\rho}{\rho_f^2 \sigma^3}$
Weber number	$We = \frac{\rho_f U d^2}{\sigma}$
Galileo number	$Ga = \frac{\rho_f^2 d^3 g}{\mu_f^2}$
Ohnesorge number	$Oh = \sqrt{\frac{We}{Re_p^2}}$
Deborah number	$De = \frac{\lambda U}{d}$
Viscosity ratio	$\eta = \mu_d/\mu_f$
Density ratio	$\beta = \rho_d/\rho_f$

Rigid particles

Direct Numerical Solution (DNS) of particle-laden turbulent flow, when $d < \eta_K$, is carried out using the two-fluid (TF) scheme or the Eulerian–Lagrangian (EL) one, where $\eta_K = \nu^{3\,1/4}/\epsilon$, $\epsilon = 2\nu\overline{S_{ij}S_{ij}}$, and $S_{ij} = \left(\frac{\partial u_i}{\partial x_j} + \frac{\partial u_j}{\partial x_i}\right)$. The main assumption of the EL procedure is based on the point particle (Elghobashi 2009). The Eulerian–Lagrangian approach is based on solving fluid flow equations in fixed gird in the Eulerian approach and solving particle dynamics in the Lagrangian approach. If $d > \eta_K$, particle is preserved as a solid body immersed in the fluid and resolved accurately (Uhlmann 2008). Hence, the resolved particle (Euler–Lagrange point-particle) approach can be employed to solve the flow field.

Point particle approach

In the point particle approach, there is a fundamental equation that describes the motion of buoyant particles in fluid flow. Obtaining a fundamental equation describing the motion of a single buoyant particle in the carrier fluid took almost a century. The resulting equation, named as Maxey–Riley equation, was derived as follows (Maxey and Riley 1983).

$$v_p \rho_p \ddot{\mathbf{X}}_p = v_p \rho_l \frac{D\boldsymbol{u}}{Dt} + \mathbf{F}_{\mathrm{MP}} + \mathbf{F}_B + \mathbf{F}_L + \mathbf{F}_D \tag{3}$$

where $v_p = \frac{\pi d_p^3}{6}$ is particle volume. To derive the Maxey–Riley equation, the effect of coupling between translation and rotation of particle has been assumed negligible. As shown in Fig. 1, the forces include the one due to the added mass $\mathbf{F}_{\mathrm{MP}} = \rho_l v_p \frac{DU}{Dt}(1 + C_M)$, drag force $\mathbf{F}_{\mathrm{D}} = -C_D \frac{\pi d_p^2}{8} \rho_l \left|\dot{X}_p - U\right| \left(\dot{X}_p - U\right)$, buoyancy force $\mathbf{F}_{\mathrm{B}} = v_p \left(\rho_p - \rho_l\right) g \hat{e}_y$ and shear-induced lift force $\mathbf{F}_{\mathrm{L}} = -C_L \rho_l v_p \left(\dot{X}_p - U\right) \times (\nabla \times U)$ (Liu et al. 2018a, b, c).

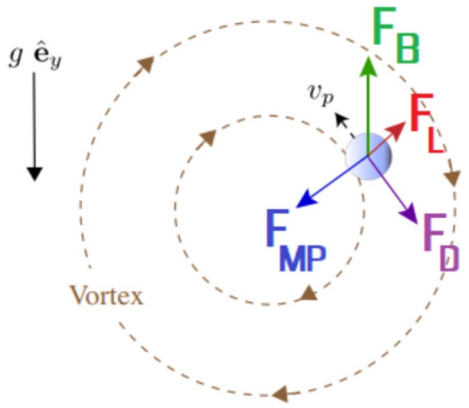

Fig. 1 Schematic of the forces applied on a small buoyant particle rising past a vortex (Liu et al. 2018a, b, c)

Two-fluid approach

When $d < \eta_K$, TF approach can be employed (Zhou 2009). In this method, the equations govern the fluid and the particulate phases are averaged spatially over $\eta_K \gg d$ (Druzhinin and Elghobashi 1998). Crowe et al. (1996) pointed out that the algorithm can be easily modified for the dispersed phase. Besides, the computational time is not as excessive as it may be for the trajectory models. Even though the TF model has good performance, its performance is strongly dependent on the closure models and computational time. By neglecting the Basset and lift forces in the Maxey–Riley equation and assuming $\rho_l \gg \rho_p$, governing equations are obtained for the particulate phase (Druzhinin and Elghobashi 1998).

Resolved particle approach

The resolved particle approach is the approach with the least simplifications. Each particle is treated as a solid body immersed in the fluid (Uhlmann 2008). The exact solution of governing equations can be obtained by determining the force of the fluid acting on the particle and vice versa. In other words, the force applied to each point of the particle's surface is calculated. The advantage of this method is its high accuracy and low computational costs. This approach is suitable when the number of particles per CPU is less than 10. Since particles and fluid have an impact on each other, their governing equations must be coupled. Depending on the volume fraction

of particles, Φ, one-way coupling (for $\Phi < 10^{-6}$), two-way coupling (for $10^{-6} < \Phi < 10^{-3}$), and four-way coupling (for $10^{-3} < \Phi < 1$) are employed. In a one-way coupling approach, the impact of fluid on the particles is considered, but the particles' effect on the fluid and inter-particle effects are negligible. In the two-way coupling approach, the carrier fluid and particles affect each other but inter-particle effects can be ignored. In a four-way coupling approach, the carrier fluid and particles affect each other. Besides, the particles have an effect on each other due to their direct collision or indirect collision due to the surrounding fluid that exists between the particles.

Deformable particles

For deformable particles when $d > \eta_K$, the interface motion is calculated using numerical methods. In the following, popular numerical approaches employed by researchers are described.

Phenomenological model

Meanwhile, current supercomputers perform DNS of the turbulent fluid flow only when $d \geq \eta_K$. Thus, the deformation of the dispersed phase is computed by using the phenomenological model. The main asset of this model is that it can be applied to an arbitrary flow. Hence, it is particularly suitable as a model of the deformable particle behavior in complex flows (Maffettone and Minale 1998).

In this model, the shape of the deformable particle is described using a second-order tensor **S**, where its evolution equation is as follows:

$$\frac{d\mathbf{S}}{dt} = \mathbf{\Omega}.\mathbf{S} + \mathbf{S}.\mathbf{\Omega} \tag{4}$$

Here, $\mathbf{\Omega} = \frac{1}{2}(\nabla \boldsymbol{u} - \nabla \boldsymbol{u}^T)$ is vorticity tensor.

Front tracking method

In this method, there is a set of governing equations is utilized for the solution area (Unverdi and Tryggvason 1992):

$$\frac{\partial \rho \boldsymbol{u}}{\partial t} + \nabla\ \rho \boldsymbol{u}\boldsymbol{u} = -\nabla P + \nabla\ \mu\left(\nabla \boldsymbol{u} + \nabla \boldsymbol{u}^T\right) + \sigma \int \kappa \boldsymbol{n} \delta^{\beta}(\boldsymbol{x} - \boldsymbol{X}) d_s \tag{5}$$

The divergence of the velocity field is zero when both immiscible fluids are incompressible:

$$\nabla\ \boldsymbol{u} = 0 \tag{6}$$

Equations of state for the density and the viscosity are:

$$\frac{D\rho}{Dt} = 0, \frac{D\mu}{Dt} = 0 \tag{7}$$

The pressure jumps across the interface, contrasting the velocity is taken to be continuous. The normal stresses are balanced by surface tension because of the continuity of stresses at the fluid boundary. The force due to surface tension is

$$\Delta \boldsymbol{F} = \sigma \kappa \boldsymbol{n} \tag{8}$$

In this approach, the interacting interfaces are accounted for, but it is expensive, even if only grid points in the vicinity of the interface are considered (Unverdi and Tryggvason 1992). The method is utilized to describe the motion of deformable particles in fluid flow (Bayareh et al. 2013).

The interface-capturing method is also introduced in the following. It utilizes continuous functions to estimate various phases. This technique can predict the topological variations. Since the indicator function of this method is different, four approaches are commonly utilized to capture the interface, including the Volume of Fluid (VOF), level-set, phase field, and Lattice Boltzmann methods.

VOF method

In the VOF method, the indicator function is selected as the volume fraction of the particles (Hirt and Nichols 1981). This method involves three major steps: the reconstruction of the interface, modeling of the advection, and estimation of the interfacial tension (Day et al. 2012). The volume fraction function is described using Eq. 6:

$$\frac{\partial \Phi}{\partial t} + \boldsymbol{u}.\nabla \Phi = 0 \tag{9}$$

The density and viscosity of the two phases are calculated using the following equations:

$$\rho(x,t) = \rho_1 \Phi + \rho_2 (1 - \Phi) \tag{10}$$

$$\mu(x,t) = \mu_1 \Phi + \mu_2 (1 - \Phi) \tag{11}$$

Here, subscripts 1 and 2 represent ambient fluid and drop, respectively. The following pattern is utilized in the VOF method:

$$\begin{cases} \Phi = 1 & \text{the cell is occupied by ambient fluid} \\ 0 < \Phi < 1 & \text{the cell includes the interface} \\ \Phi = 0 & \text{the cell is occupied by drop} \end{cases} \tag{12}$$

The interfacial tension force is calculated by using the continuum surface force (CSF) scheme (Brackbill et al. 1992). The normal vector and curvature of the interface are calculated using the derivatives of the volume fraction function or models. The VOF method is easy to extend to three-dimensional problems, has high accuracy, and is simple to implement (Cannon et al. 2021).

Level set method

The level set method is also described by using the following equation:

$$\frac{\partial \Phi}{\partial t} + \boldsymbol{u}.\nabla\Phi = 0 \tag{13}$$

In this method, $\Phi = 0$ at the interface. The indicator function of this method is a smooth function that represents the interface in the computational domain and does not have any physical meaning (Olsson and Kreiss 2005). Because of smoothed changes across the interface, discontinuity does not happen. This method needs a significant attempt to determine applicable velocities to proceed with the level set function, which can break the mass conservation law for each phase (Sussman and Fatemi 1999; Balcázar-Arciniega et al. 2019).

Phase-field method

The indicator function of this method is the density function of one phase (Santra et al. 2020), leading to the satisfaction of the continuity equation. The interface transport equation is described in Eq. 8 (Cahn and Hilliard 1958):

$$\frac{\partial \theta}{\partial t} + \boldsymbol{u}.\nabla\varphi = \nabla.(M\nabla\varphi) \tag{14}$$

This method retains the interface sharpness while the continuity is maintained [46]. Because of this property and since no more attempts are required to reconstruct the interface and re-initialize the time step, this method is a favorite for simulation of interaction and coalescence between deformable particles (Liu et al. 2021).

Lattice Boltzmann method

This technique is in accordance with the discretized fluid model of Lattice Gas Automata (LGA) (Liu et al. 2021) and basically tracks the evolution of the probability distribution function for particles in a discretized space and time domain (Liu et al. 2021). One of the significant parameters in the lattice Boltzmann method, such as Shan and Chen model (Shan, and Chen 1993) is the discretization of the force terms due to the creation of numerical instabilities. Some researchers proposed stable models to describe the two-phase flows, for instance, Lee and Lin (2005) suggested a stable lattice Boltzmann model for high density and viscosity ratios. Discretization errors cause parasitic velocities in the vicinity of the interface when external forces are not applied. Numerical instability is enhanced by intensifying the parasitic velocities and surface tension. To diminish parasitic velocities, the pressure gradients and the term involves surface tension can be modified or the sharp interface technique may be utilized (Wagner 2003). Hence, the LBM is useful, especially for deformable particles (Tiribocchi et al. 2020). Several commercial software applications, such as ANSYS FLUENT, COMSOL Multiphysics, Floe-3D, STAR-CD, STAR-CCM, etc., can be employed to simulate two-phase flow problems.

Figure 2 summarizes various approaches that can be utilized to simulate the motion of rigid and deformable particles in a fluid flow.

Configuration of deformable particles

The description of particle-laden flows is important for the design and operation of industrial applications. The complexity of collision dynamics of particles is a challenge and many numerical and experimental investigations have been done to describe this phenomenon. Compared to rigid particles, the internal fluid circulation of deformable particles leads to their different behavior. They can be classified into double emulsions and bubbles/drops. Double emulsions show similar trajectories and different deformation during their interaction in comparison with the deformable drops with a single phase (Liu et al. 2018a, b, c). Three colliding modes were observed for two eccentric double emulsions: merging, passing over and reversing (Nguyen and Vu 2020). The competition between the drag of the passing-flow region and the entrainment from reversing-flow and vortex regions in the matrix fluid determines the colliding type.

Hydrodynamic behaviors of double emulsions under the influence of an external flow describe the differences between their collision and the binary interaction of single-phase drops. Besides, the impact of the inner-outer radius ratio on the colliding dynamics can be realized (Liu et al. 2018a, b, c). Moreover, simulation of colliding phenomena of two single-core compound droplets in simple shear flow showed that Reynolds number, the viscosity ratios μ_{1-3} and μ_{2-3}, the interfacial tension ratio $\sigma_{1 \text{ and } 2}$, and the initial distance between two droplets affect the colliding motion (Vu 2019) (Fig. 3). Indices 1 and 2 represent the inner droplets and index 3 shows the ambient fluid. Rotation and the eccentricity of the double emulsions affect the type of collision modes. In simple shear flow, the impact of the location of the inner droplet in the outer one is considerable when $0.01 < Ca < 0.08$. For $Ca < 0.01$ and $Ca \geq 0.16$, the location of the inner droplet does not affect the interaction dynamics of double emulsions (Nguyen and Vu 2020).

The collision of two eccentric drops in the Couette flow may follow the drafting-kissing-tumbling (DKT) phenomenon (Balcázar- Arciniega et al. 2019) (Fig. 4). In the drafting step, the wake formed by the leading droplet

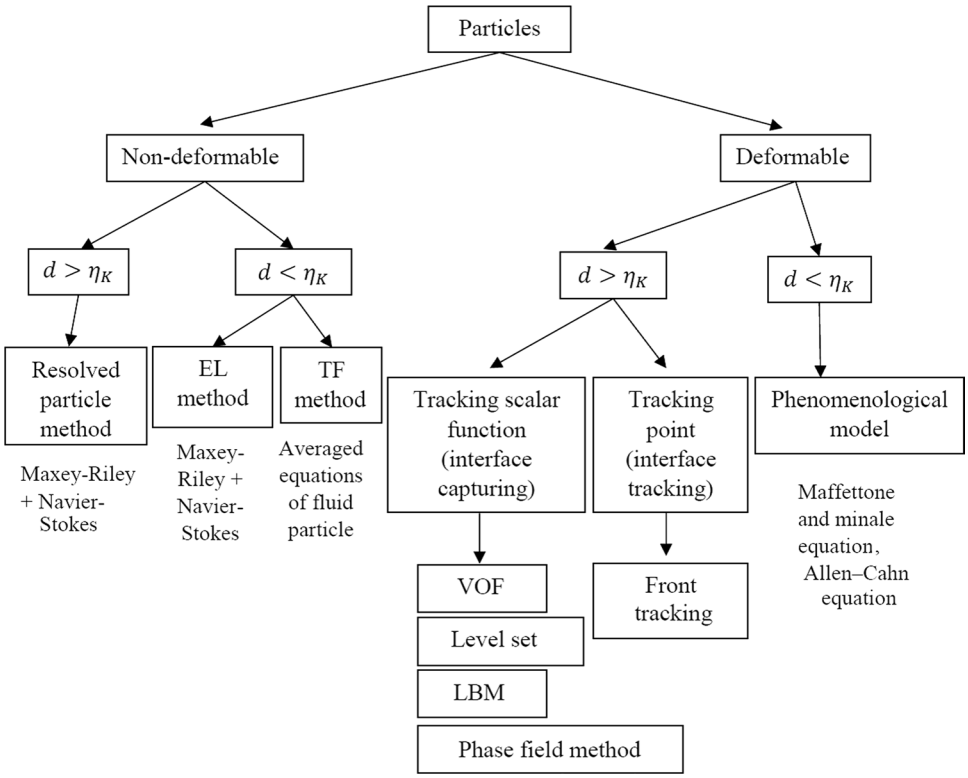

Fig. 2 Classification of numerical methods based on the deformability and size of particles (Elghobashi 2009; Zhou 2009; Maffettone and Minale 1998; Unverdi and Tryggvason 1992; Hirt and Nichols 1981; Olsson and Kreiss 2005; Santra et al. 2020; Benzi et al. 1992; Khan et al. 2020; Gobert and Manhart 2011)

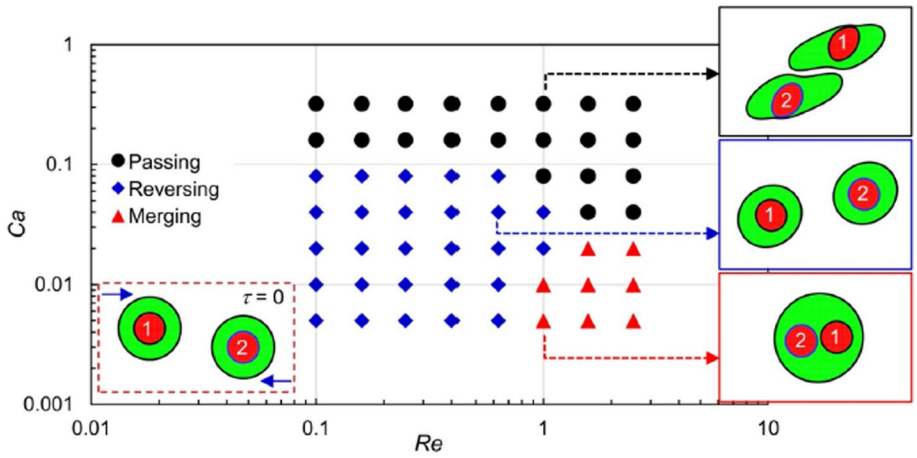

Fig. 3 Three collision modes of two single-core compound droplets (Vu 2019): $Re_{12} = 0.5$, $\mu_{13} = \mu_{23} = 1.0$, $\Delta x_o/R_2 = 3.0$, and $\Delta y_o/R_2 = 0.6$, where Δx_o and Δy_o are center-to-center distance of droplets in x- and y-direction, respectively, and subscripts 3 indicates the ambient fluid

quickens the movement of the trailing one until it contacts the leading one. Then, they slide around each other during the tumbling step. Finally, they interact with the wall due to the bouncing impact. DKT process observed for the swarm of drops results in the creation of clusters moving in the channel centerline (Bayareh and Mortazavi 2009; Bayareh and Mortazavi 2011). We, Re, η, β, and size of droplets/bubbles determine the binary collision mode moving in a horizontal channel (Goodarzi et al. 2018). In a head-on collision of two drops in a vertical channel, when We and Re increase, the deformation of drops enhances, and gap thickness decreases. Higher density ratios result in the drops colliding with each other faster. An increment in We and Re and a reduction in η result in an enhancement in the elongation of drops (Hassanzadeh et al. 2019).

Even though the interaction between two off-center particles has been considered in previous articles, many investigators have analyzed two specific types of configuration to describe the collision dynamics of particles, including in-line and side-by-side arrangements.

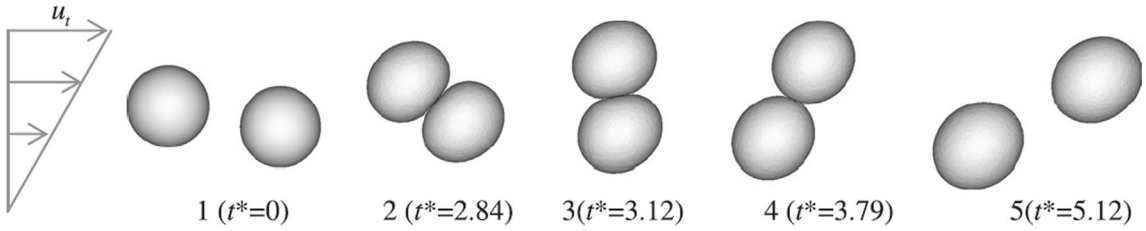

Fig. 4 DKT phenomenon in simple shear flow: Re_b= 10, Ca = 0.13, and $\eta = 1$ at different dimensionless times (Bayareh and Mortazavi 2011)

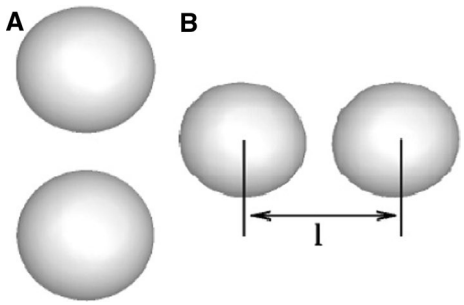

Fig. 5 **A** In-line and **B** side-by-side configurations

In-line configuration

The significance of vertical ordering (Fig. 5A) is higher than the horizontal one since vertical arrangement results in the creation of vertical chains in deposition (Joseph et al. 1994). Arrangement of particles influences collision dynamics. DKT phenomenon occurs in the collision of two spheres ascending with in-line ordering in a homogenous fluid (Bayareh et al. 2013). Two deformable rising or falling drops in an in-line configuration may attract each other due to viscoelastic normal stresses (Zenit and Feng 2018). Two in-line drops moving in a linearly stratified fluid keep their arrangement (Dabiri et al. 2015). In the case of rising bubbles in an in-line ordering, the trailing one is prone to speed up beyond its terminal velocity. The bubbles hit and coalesce due to their velocity difference at low Reynolds numbers. At higher Reynolds numbers, due to vorticity evolution about the trailing bubble, deviation away from the in-line configuration occurs (Gumulya et all. 2017). Under different confinement ratios, two initially spherical in-line buoyant bubbles can coalesce (Gui et al. 2020). The co-axial coalescence phenomenon for two in-line bubbles at low values of Re involves coalescence with and without a conjunction. In the last one, the thinning velocity of the liquid film is decreased with time. In conjunct coalescence, the bubbles slide on each other as the liquid viscosity decrease or a surfactant is added (Feng et al. 2016).

Side-by-side configuration

Comprehensive experiments were performed by Joseph et al. (1994) for two side-by-side particles (Fig. 5B). Two deformable rising or falling drops in a side-by-side order, attract each other due to the normal stress effect, in a viscoelastic fluid (Zenit and Feng 2018). Two nearly spherical drops ascending side by side retain their initial arrangement; however, the separation distance is reduced after their preliminary hit (Dabiri et al. 2015). Motion and interaction of three parallel equal-sized bubbles showed that coalescence or repulsion depends on physical parameters [54]. By changing the radius of the bubble and center-to-center distance between two identical air bubbles rising side by side in the water, the collision dynamics between the two bubbles is changed. Besides, an increment in the size of the bubbles leads to a smaller terminal velocity (Meenu Agrawal et al. 2021). Hydrodynamic collision of side-by-side spheres indicted that lift and drag coefficients depend on their separation distance. At slippery spheres facing each other, the repulsion behavior changes to the coalescence regime by increasing the Reynolds number (Dhiman et al. 2021). Compared to a single drop, the sensitivity of a pair of side-by-side ones to viscosity is smaller. Also, an increase in the density ratio leads to a non-monotonic trend in the separation distance between the drops (Balla et al. 2020).

Fluid flow types

Shear flow

One of the most widely used fluid flows to analyze two-phase flows is shear flow, the flow between two parallel plates or two coaxial co- or counter-rotating cylinders (Dhiman et al. 2021). Soligo et al. (2020) investigated demonstrated that the surface tension and surfactant play a main role in the droplet deformation, whereas tangential stresses have a slight impact. Chen et al. (2015) studied the dynamics of double emulsion droplets in Couette flow experimentally and numerically. They focused on transient deformation topologies and demonstrated that the inner droplet intensifies

the retracting of the outer one and provided a regime diagram for their deformation based on Ca and the ratio of inner droplet radius to the outer one. Liu et al. (2018a, b, c) simulated hydrodynamic shear-driven binary collision of double emulsion droplets. Vu et al. (2019) investigated the influences of different factors and numbers of the inner droplets encapsulated in the compound droplet on the deformation and breakup of the multi-core double emulsions in the shear flow. Dynamic behavior of emulsion with multi-core morphology in shear flow showed that the emulsion exhibits a solid-like behavior under low shear rates. By increasing the shear rate, two steady states may occur: (i) inner cores align along with the flow, and (ii) some cores gather in the vicinity of the outer interface and generate a ring chain and others occupy the center of the emulsion (Tiribocchi et al. 2020).

Rheology of a dense suspension of spherical capsules in simple shear flow in the Stokes flow regime was described by Matsunaga et al. (2015) using a polynomial equation of the volume fraction. They revealed that the effect of higher-order terms is much smaller for capsule suspensions than rigid sphere suspensions. It was found that as the volume fraction enhances, the capsule deformation is increased. Also, Zhu and Gallairs (2017) studied the dynamics of a particle-encapsulating droplet in shear flow by considering the effect of the surface tension between the outer and the inner interfaces. For a moderate capillary number, the large inner droplet could promote the detachment and the acceleration of the pinch-off process is increased with the lateral migration of the small inner droplet (Shang et al. 2019). The evolution of the size distribution of an emulsion under a simple shear flow is important. A broad single-peak distribution of drops is observed and the rupture of drops occurs at higher shear rates. The evolutions showed global structures such as "pearl necklaces" and "bands of particles" (Leiva and Geffroy 2018). For an initially ellipsoidal compound capsuled, the transition from swinging to tumbling enhances the inner capsule size and critical viscosity ratio for the swinging-to-tumbling transition (Luo and Bai 2016). Effect of surface tension coefficient, viscosity ratio, and inertia on lateral migration and deformation of a spheroidal deformable drop revealed that the Reynolds number increases the slip velocity; hence, the prolate drops reach faster the equilibrium position at low Reynolds numbers (Armandoost et al. 2018).

The spatial cross-correlated diffusion of colloids is employed to describe the hydrodynamic interaction between two particles in a fluid. Li et al. (2018) examined the effect of shear flow on spatial cross-correlated diffusion and showed a dependence on pair angles. Dynamics of a rigid sphere in inertial shear flow between parallel walls (horizontal and vertical) demonstrated that bifurcation will break and a single off-center equilibrium position is achieved at various particle Reynolds numbers and sufficiently strong gravitational force (Fox et al. 2021). Rosti and Brandt (2018) studied suspensions of deformable particles in a shear flow. They analyzed the rheology of the suspension by studying the effect of changes in the particle volume fraction Φ, Ca, and the solid-fluid viscosity ratio K on viscosity μ and observed that μ is a nonlinear function of these parameters, i.e., $\mu = \mu(\Phi, Ca, K)$. Bayareh and Mortazavi (2012) showed that the equilibrium position of the lighter drops is higher than the heavier ones at each particle Reynolds number.

Poiseuille flow

Poiseuille flow can be described by solid volume fraction, Re, and Ca. For a suspension of deformable particles, the effect of these parameters on effective viscosity was investigated (Chiara et al. 2020). At high shear rates, effective viscosity is reduced, leading to a shear-thinning action. The dependence of viscosity to Re is higher than Ca. Where the shear rate is low, deformable particles move towards the center of the channel. Also, particles are more sensitive to shear rate variations and can recover their shape more easily (Chiara et al. 2020). The hydrodynamics of double emulsions in a Poiseuille flow revealed that the core affects the drop dynamics only at intermediate sizes (Gurumurthy and Pushpavanam 2020). For large sizes, the deformation of the double emulsions is nearly the same as the simple drop (Karp et al. 2021). The equilibrium position of a deformable drop, when the drop is slightly buoyant, is between the wall and the channel centerline (Bayareh and Mortazavi 2012). A large viscosity ratio makes the droplet located in a near-wall equilibrium position, and a large capillary number makes the droplet migrate to the near-centerline region of the channel (Pan et al. 2016). It was known that viscosity has a major impact on the droplet migration rate (Das and Chakraborty 2018).

Stratified flow

A stratified fluid is described as a fluid with density variations in the vertical direction. Cooray et al. (2017) investigated the dynamics of interacting particles moving through sharp interfaces. Dabiri et al. (2015) presented the rising motion of drops in a linearly stratified fluid. Bayareh et al. (2016) investigated two drops with in-line and side-by-side arrangements in a linearly stratified fluid. During the interaction of side-by-side drops, they retain in the horizontal ordering and after their initial collision, the rate of separation is decreased. Also, for the in-line configuration, drops move in tandem and remain their configuration (Fig. 6). Rising dynamics of a deformable drop in a linearly stratified fluid demonstrated the effect of drag coefficient of a spherical drop, buoyancy induced vortices, and the resultant buoyant jet. Studying the behavior of a circular disk in a linearly stratified fluid showed that when a disk reaches its

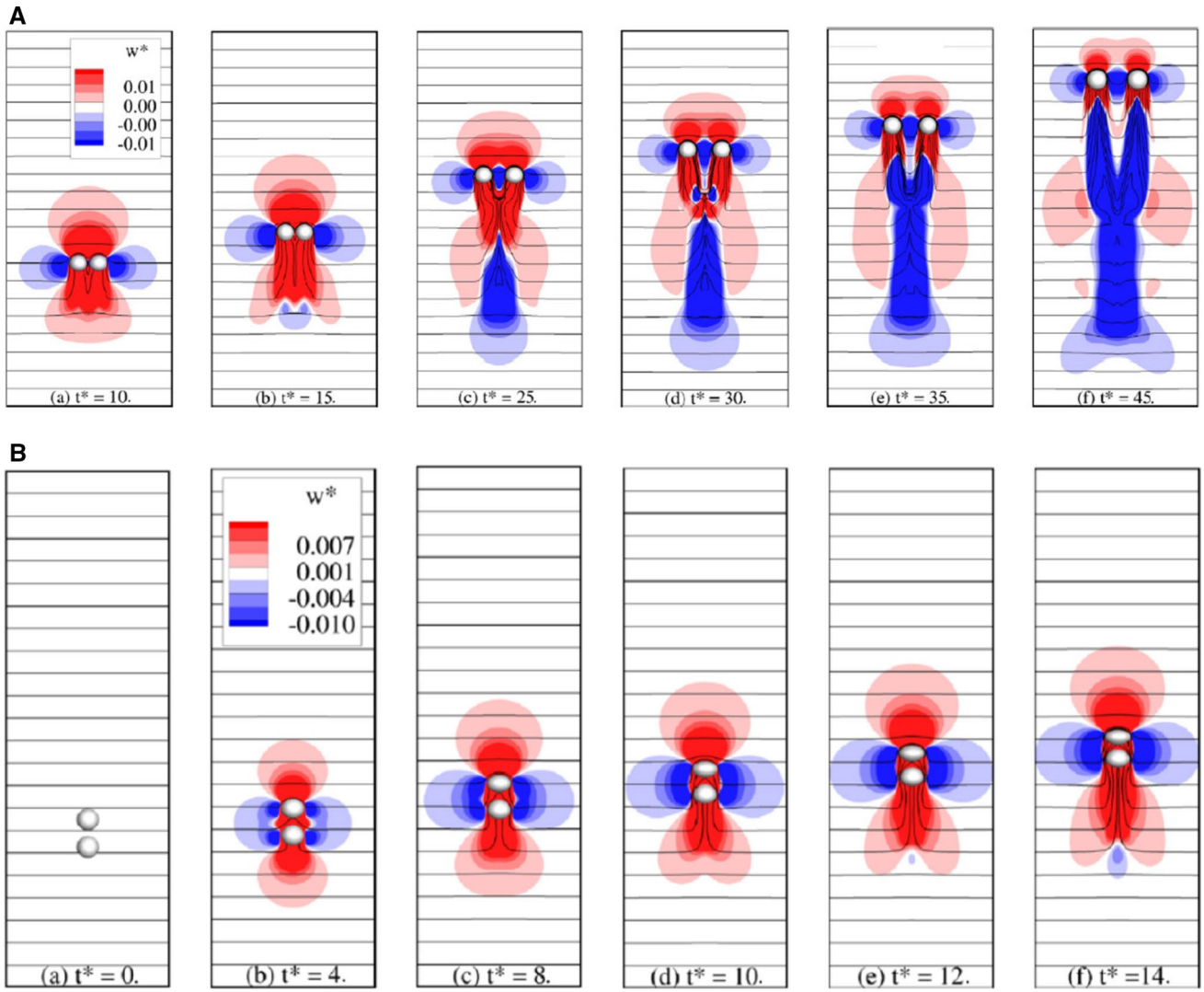

Fig. 6 Rising motion of two drops in a linearly stratified fluid: **A** side-by-side configuration and **B** in-line configuration (Bayareh et al. 2016)

gravitational equilibrium level, there are three regimes for the settling dynamics, including broadside-on, edgewise, and returning to its broadside orientation (Mercier et al. 2019). When a drop is settled in stratified flow, core mechanisms enhance the drag (Zhang et al. 2019). The density, viscosity, and surface tension of the two liquids, bubble diameter, Weber and Morton numbers are the effective parameters of bubble interaction. Changing these parameters and dynamics of air bubbles can create three flow regimes, including penetration flow regime, entrainment flow regime, and envelopment flow regime (Farhadi et al. 2021).

Fluid flow driven by an external force

Fluid flow can be driven by magnetic force, electric force, electromagnetic force, etc. Some investigators evaluated the impact of the electric force on the dynamics of drops. The electric field can change the deformation and orientation of a neutrally buoyant drop (Mandal and Chakraborty 2017). For example, the deformation of a drop is changed due to the combined influence of an applied electric field and shear flow (Borthakur et al. 2021). By applying an electric field, the orientation angle of a drop may either increase or decrease. In the absence of an electric field, the orientation angle decreases with the degree of confinement (Santra et al. 2019a, b). In a Poiseuille flow, applied transverse electric field affects pinch-off dynamics of a double emulsion. The strength of the electric field, as well as the electric properties of the fluids, influences the temporal evolution of drop eccentricity and the kinetics of the thinning of the outer one (Santra et al. 2019a, b).

Extensional flow

The simplest definition of an extensional flow is the deformation that involves stretching along streamlines. The drop deforms gradually from prolate spheroid to "peanut" in uniaxial extensional flow, or from oblate spheroid to "red-blood-cell" in biaxial extensional flow (Liu et al. 2018a, b, c). Mechanical mechanisms of the directional movement and inverse of an eccentric compound droplet in extensional flow showed that the directional shift and inverse of the compound droplet are due to the interaction of the inner driving force (curvature difference) and the outer drags (Wang et al. 2018). The oriented shift and inverse of double-emulsion globules involving two inner drops with different sizes and locations in an extensional flow were evaluated by Xu et al. (2017). They demonstrated that asymmetric rheological behavior may occur because the asymmetric layout of daughter droplets leads to the asymmetric inner flow field and pressure field inside the globule. Analysis of the interaction of the inner and outer interfaces of a surfactant-covered double emulsion was performed by considering the effect of Péclet number (Pe) and Ca. It was shown that the outer drop deformation is enhanced and the inner drop deformation is reduced when the surfactant is employed (Lee et al. 2020). As Ca and Pe are enhanced, the surfactant concentration at the outer interface is intensified and the deformation of the inner drop decreases.

Non-newtonian fluid

Many fluids containing particles are non-Newtonian (Zenit and Feng 2018). Exact approximations and semi-empirical models are employed to model non-Newtonian fluid flows. Here, semi-empirical models, including the generalized Newtonian ones and the Oldroyd-B model, are described. The generalized Newtonian models are the same as the Newtonian ones, however, the viscosity is estimated as a function of the shear rate, $\dot{\gamma}$:

$$\boldsymbol{\tau} = -p\mathbf{I} + 2\mu(\dot{\gamma})\mathbf{E} \tag{15}$$

Where

$$\dot{\gamma} = \sqrt{2\mathbf{E} : \mathbf{E}} \tag{16}$$

Some common statements for the viscosity are as follows: Power-law non-Newtonian fluids (Waele 1923):

$$\mu(\dot{\gamma}) = \kappa'\dot{\gamma}^{n-1} \tag{17}$$

Carreau-Yasuda non-Newtonian fluids (Yasuda and Cohen 1981):

$$\mu(\dot{\gamma}) = \mu_\infty + \left(\mu_o - \mu_\infty\right)\left[1 + (\lambda\dot{\gamma})^a\right]^{\frac{n-1}{a}} \tag{18}$$

The Oldroyd-B model is one of the simplest models that involves the flow history (Oldroyd 1950) and its form can be expressed as

$$\boldsymbol{\tau} = -p^*\mathbf{I} + 2\mu^*\mathbf{E} + \frac{G}{\lambda_1}\mathbf{A} \tag{19}$$

Where $p^* = p + 2\left(1 - \lambda_2/\lambda_1\right)\mu/\lambda_1$, $\mu^* = \mu\lambda_2/\lambda_1$, and $G = 2\left(1 - \lambda_2/\lambda_1\right)\mu$.

Literature reviews designate that the rheological characteristics of the continuous phase have a strong impact on the rigid/deformable particle behavior (Moosaie et al. 2015). The drop deformation in the Newtonian fluid is less than that in non-Newtonian ones. D'Avino and Maffettone (2015) presented a review of solid particles depositing in viscoelastic liquids. They investigated the dynamics of non-Brownian particles in viscoelastic fluid. The motion of a Taylor drop in a non-Newtonian fluid was examined by Usefi and Bayareh (2020). They studied the effect of Eö and Fr on the behavior of a Taylor drop. Increasing the power-law index due to increasing Froude number leads to an increment in the thickness of the thin layer of the fluid about the drop. Also, inelasticity affects the migration of a drop and the interaction of two drops. In Couette flow, inelasticity results in drop deformation and a reduction in the migration rate of drops. For an inelastic system, in comparison with the Newtonian one, the time of the collision process is shorter (Masiri et al.

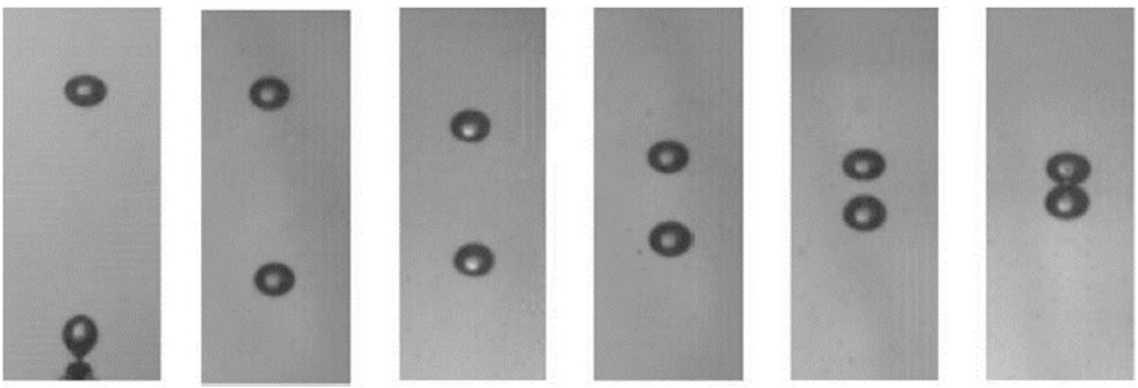

Fig. 7 Coalescence of two bubbles rising in an in-line configuration in shear-thinning non-Newtonian fluid (Sun et al. 2017)

Table 2 Some investigations performed on binary collision of deformable particles

Configuration of particles	Fluid flow	Dimensionless parameters	Numerical simulation	Results	Refs.
Off-center binary collision	Clean and surfactant drops in shear flow	$0.0625 < Ca < 0.250$	Phase field method	The occurrence of coalescence and non-coalescence modes depends on surfactant bulk concentration, elasticity number, and Ca	Soligo et al. (2019)
Off-center binary collision	Clean drops in shear flow	$Ca = 0.3$ $Re = 1$	LBM	Breakup and coalescence of drops depends on Ca, Re, and their initial position	Takada et al. (2003)
In-line and side-by-side collision	Rising bubbles in stagnant liquid	Re ~ 30 (parallel bubbles) and 60 (in-line bubbles)	VOF and CSF	Coalescence occurs for both configurations	Sun et al. (2019)
Binary collision of double emulsion drops	Shear flow	$0.05 < Ca < 0.4$	VOF	Two regimes are observed: passing-over and reversing motion. These regimes depend on Ca and confinement degree of shear flow	Liu et al. (2018a, b, c)
Off-center compound drops	Shear flow	$0.005 < Ca < 0.04$ $0.01 < Re < 10$	Front tracking	Tree regimes are observed: merging, passing-over, and reversing motion. These regimes depend on Ca and Re	Vu (2019)
Eccentric compound drops	Shear flow	$0.005 < Ca < 0.32$ $Re = 1.6$	Front tracking	Tree regimes are observed: merging, passing-over, and reversing motion. These regimes depend on Ca and Re	Nguyen and Vu (2020)
Off-center binary collision	Shear flow	$0.05 < Ca < 0.3$ $Re = 10$	Front tracking	DKT phenomenon occurs for the range of Ca studied. The trajectories of drops become more symmetric by increasing viscosity ratio.	Bayareh and Mortazavi (2011)
Off-center binary collision of water drops	The drops have different initial velocity	$0.53 < We < 2.126$ $26 < Re < 107$	VOF	The drop elongation depends on β, η, We, and Re	Bayareh and Mortazavi (2009)
Two bubbles rising in an in-line configuration	Stagnant fluid	$< Eo < 1$ $Re < 890$	VOF	The inline configuration of the two bubbles is stable at low values of Re. At $Re > 50$, the bubble deviates away from the rectilinear path.	Gumulya et al. (2017)
Collision of two in-line bubbles	Stagnant fluid	$1.7 < Mo < 660$ $0.7 < Re < 1.2$	VOF	Conjunct rising and conjunct coalescence are observed that depend on the Re of the two bubbles	Feng et al. (2016)

Table 2 (continued)

Configuration of particles	Fluid flow	Dimensionless parameters	Numerical simulation	Results	Refs.
Two drops rising side by side	Quiescent surrounding medium	Ga = 20 and 50 Eo ~ 4	VOF	Two bubbles tend to separate as they rise at low Ga. For Ga = 20, bubbles display three-dimensional motion and the separation between the bubbles increases.	Balla et al. (2020)
Two in-line and side-by-side drops	Linearly stratified fluid	Eo = 0.64 and 3 Fr = 11 and 22 Re = 790	Front tracking	Two in-line drops moving in line retain their configuration. Two side-by-side drops remain in the horizontal alignment.	Bayareh et al. (2016)
Two in-line bubbles	Shear-thinning non-Newtonian fluid	2 < Re < 60	Experimental work	The minimum coalescence height of bubbles is reduced by enhancing the mass concentration of the ambient solution.	Sun et al. (2017)

2019). At high inelasticity, two Newtonian drops in an elastic simple shear flow exhibit reversible cross-flow migration. Based on the dynamics of bubble rise in Bingham fluids, the bubble achieves a constant rise velocity in weak yield stress. By enhancing yield stress, the bubble rise is unsteady and the aspect ratio oscillates above a value that exceeds unity (Tripathi et al. 2015a, b). The rising motion of bubbles with an equilateral triangle arrangement in shear-thinning fluids showed that bubbles' size, their formation frequency, their preliminary distance, and liquid property affect the collision mechanism. The decrease in initial bubble distance and the increase in bubble diameter lead to the decrease in drag coefficient [24]. A study on a rising air bubble in a shear-thinning non-Newtonian fluid demonstrated that Galileo and Eo affect the dynamics of the bubble. At Ga = 30 and Eo = 1, the deformation and vortex shedding during the wobbling (zigzagging/spiraling) motion was observed, and at Eo =25, the bubble experiences peripheral break-up. Bubble behavior was identified in five different regions [112]. The dynamic of the bubble was investigated in these five regions (Sharaf et al. 2017). Liu et al. (2015) presented the effects of bubble size, rheological properties of shear-thinning fluids, and orifice structure arrangements on dynamics of interaction, coalescence, and the breakup of multiple bubbles. Deformation dynamics of a moving double emulsion inside a micro-capillary tube showed that the location of inner and outer drops is enhanced linearly in a Newtonian fluid, whereas this is nonlinear for a non-Newtonian one (Sattari et al. 2021). Investigation of in-line coalescence height of bubbles in shear-thinning non-Newtonian fluid at lower Reynolds number showed that when the nozzle diameter and gas flow rate increase, minimum in-line coalescence height is reduced (Fig. 7) (Sun et al. 2017). In non-spherical particle-laden flow, the rheology of a dilute suspension of Brownian thin disk-like demonstrated that thinner disks create higher stresses than thicker disks, and shear viscosity of the suspension is more important than its extensional viscosity (Moosaie et al. 2017).

Concluding remarks and future trends

The current paper provides a review of the binary collision of deformable particles. Numerical approaches to simulate the motion of two interacting particles are presented and the impact of deformability and initial configuration of deformable particles as well as flow type on collision dynamics is examined. It is concluded that dimensional parameters, including Ca, Eo, Re, Mo, β, and η, and configuration and type of surrounding medium determine the behavior of interacting drops/bubbles. Table 2 provides the details of some investigations performed on binary collision of deformable particles.

Despite a huge number of researches carried out on multiphase flow laden with deformable particles, numerous gaps and challenges still exist. For example, due to the complexity and large-scale computation of numerical methods, the interaction between double emulsions has not been considered in sharp and linearly stratified fluids. Besides, there is no experimental investigation to describe the collision dynamics of two compound drops in non-Newtonian and stratified fluids. Most numerical simulations have been performed for a small range of dimensionless parameters, such as Ca or Re. Characteristic diagrams can be provided in the future for a wider range of non-dimensional parameters and different surrounding mediums.

References

Acrivos A (1983) The breakup of small drops and bubbles in shear flows. Ann N Y Acad Sci 404:1–11

Acrivos A, Lo TS (1978) Deformation and breakup of a single slender drop in an extensional flow. J Fluid Mech 86:641–672

Armandoost P, Bayareh M, Ahmadi Nadooshan A (2018) Study of the motion of a spheroidal drop in a linear shear flow. J Mech Sci Technol 32:2059–2067

Balcázar-Arciniega N, Rigola J, Oliva A (2019) DNS of mass transfer from bubbles rising in a vertical channel. Lect Notes Comput Sci 11539:596–610

Balla M, Kavuri S, Tripathi MK, Sahu KC, Govindarajan R (2020) Effect of viscosity and density ratios on two drops rising side by side. Phys Rev Fluids. https://doi.org/10.1103/PhysRevFluids.5.013601

Barthes-Biesel D, Acrivos A (1973) Deformation and burst of a liquid droplet freely suspended in a linear shear field. J Fluid Mech 61:1–22

Bayareh M, Mortazavi S (2009) Geometry effects on the interaction of two equal-sized drops in simple shear flow at finite reynolds numbers. 5th International Conference: Computational methods in multiphase flow. WIT Trans Eng Sci 63:379–388

Bayareh M, Mortazavi S (2011) Binary collision of drops in simple shear flow at finite reynolds numbers. Adv Eng Softw 42:604–611

Bayareh M, Mortazavi S (2013) Equilibrium position of a buoyant drop in couette and poiseuille flows at finite reynolds numbers. J Mech 29:53–58. https://doi.org/10.1017/jmech.2012.109

Bayareh M, Doostmohammadi A, Dabiri S, Ardekani AM (2013) On the rising motion of a drop in stratified fluids. Phys Fluids 25:23029

Bayareh M, Dabiri S, Ardekani AM (2016) Interaction between two drops ascending in a linearly stratified fluid. Eur J Mech 60:127–136

Benzi R, Succi S, Vergassola M (1992) The lattice Boltzmann equation: theory and applications. Phys Rep 222:145–197

Besagni G, Inzoli F, Ziegenhein T (2018) Two-phase bubble columns: a comprehensive review. Chem Engineering 2:1–80

Borthakur MP, Nath B, Biswas G (2021) Dynamics of a compound droplet under the combined influence of electric field and shear flow. Phys Rev Fluids 6:23603

Brackbill JU, Kothe DB, Zemach C (1992) A continuum method for modeling surface tension. J Comput Phys 100:335–354

Busuke H, Tatsuo T (1969) Two-dimensional shear flows of linear micropolar fluids. Int J Eng Sci 7:515–522

Cahn JW, Hilliard JE (1958) Free energy of a nonuniform system I interfacial free energy. J Chem Phys 28:258–267

Cannon I, Izbassarov D, Tammisola O, Brandt L, Rosti ME (2021) The effect of droplet coalescence on drag in turbulent channel flows. Phys Fluids 33(8):085112. https://doi.org/10.1063/5.0058632

Chen Y, Liu X, Zhao Y (2015) Deformation dynamics of double emulsion droplet under shear. Appl Phys Lett 106:141601

Chen Z, Xu J, Wang Y (2019) Gas-liquid-liquid multiphase flow in microfluidic systems – a review. Chem Eng Sci 202:1–14

Chiara LF, Rosti ME, Picano F, Brandt L (2020) Suspensions of deformable particles in poiseuille flows at finite inertia. Fluid Dyn Res 52:65507

Chin HB, Han CD (1980) Studies on droplet deformation and breakup. II. breakup of a droplet in nonuniform shear flow. J Rheol 24:1–37

Cooray H, Cicuta P, Vella D (2017) Floating and sinking of a pair of spheres at a liquid–fluid interface. Langmuir 33:1427–1436

Crowe CT, Troutt TR, Chung J (1996) Numerical models for two-phase turbulent flows. Annu Rev Fluid Mech 28:11–43

Dabiri S, Doostmohammadi A, Bayareh M, Ardekani AM (2015) Rising motion of a swarm of drops in a linearly stratified fluid. Int J Multiph Flow 69:8–17

Das S, Chakraborty S (2018) Influence of complex interfacial rheology on the thermocapillary migration of a surfactant-laden droplet in poiseuille flow. Phys Fluids 30:22103

D'Avino G, Maffettone PL (2015) Particle dynamics in viscoelastic liquids. J Nonnewton Fluid Mech 215(80–104):2015

Dhiman M, Gupta R, Reddy KA (2021) Hydrodynamic interactions between two side-by-side Janus spheres. Eur J Mech B/Fluids 87:61–74

Ding S, Serra CA, Vandamme TF, Yu W, Anton N (2019) Double emulsions prepared by two–step emulsification: history, state-of-the-art and perspective. J Control release 295:31–49

Druzhinin OA, Elghobashi S (1998) Direct numerical simulations of bubble-laden turbulent flows using the two-fluid formulation. Phys Fluids 10:685–697

Elghobashi S (2019) Direct numerical simulation of turbulent flows laden with droplets or bubbles. Annu Rev Fluid Mech 51:217–244. https://doi.org/10.1146/annurev-fluid-010518-040401

Feng J, Li X, Bao Y, Cai Z, Gao Z (2016) Coalescence and conjunction of two in-line bubbles at low Reynolds numbers. Chem Eng Sci 141:261–270

Friedlander SK (1961) A note on transport to spheres in Stokes flow. AIChE J 7:347–348

Gobert C, Manhart M (2011) Subgrid modelling for particle-LES by spectrally optimised interpolation (SOI). J Comput Phys 230:7796–7820

Goodarzi Z, Ahmadi Nadooshan A, Bayareh M (2018) Numerical investigation of off-centre binary collision of droplets in a horizontal channel. J Brazilian Soc Mech Sci Eng. https://doi.org/10.1007/s40430-018-1075-y

Gui Y, Shan C, Zhao J, Wu J (2020) Wall effect on interaction and coalescence of two bubbles in a vertical tube. AIP Adv 10:105210

Gumulya M, Utikar RP, Evans GM, Joshi JB, Pareek V (2017) Interaction of bubbles rising inline in quiescent liquid. Chem Eng Sci 166:1–10

Gurumurthy VT, Pushpavanam S (2020) Hydrodynamics of a compound drop in plane poiseuille flow. Phys Fluids. https://doi.org/10.1063/5.0009401

Hassanzadeh M, Ahmadi Nadooshan A, Bayareh M (2019) Numerical simulation of the head-on collision of two drops in a vertical channel. J Brazilian Soc Mech Sci Eng. https://doi.org/10.1007/s40430-019-1624-z

Hirt CW, Nichols BD (1981) Volume of fluid (VOF) method for the dynamics of free boundaries. J Comput Phys 39:201–225

Ioannou N, Liu H, Zhang YH (2016) Droplet dynamics in confinement. J Comput Sci 17:463–474
Joseph DD, Liu YJ, Poletto M, Feng J (1994) Aggregation and dispersion of spheres falling in viscoelastic liquids. J Nonnewton Fluid Mech 54:45–86
Karp JR, Mancilla E, da Silva FS, Legendre D, Zenit R, Morales REM (2021) The dynamics of compound drops at high reynolds numbers: drag, shape, and trajectory. Int J Multiph Flow 142:103699
Khan SA, Shah A, Saeed S (2020) Numerical simulation of the interaction between three equal-sized rising bubbles using the phase-field method. AIP Adv. https://doi.org/10.1063/1.5144963
Lee T, Lin CL (2005) A stable discretization of the lattice Boltzmann equation for simulation of incompressible two-phase flows at high density ratio. J Comput Phys 206:16–47
Lee HM, Bin Choi S, Kim JH, Lee JS (2020) Interfacial behavior of surfactant-covered double emulsion in extensional flow. Phys Rev E 102:53104
Li N, Zhang W, Jiang Z, Chen W (2018) Spatial cross-correlated diffusion of colloids under shear flow. Langmuir 34:10537–10542
Liu J, Zhu C, Wang X, Fu T, Ma Y, Li H (2015) Three-dimensional numerical simulation of coalescence and interactions of multiple horizontal bubbles rising in shear-thinning fluids. AIChE J 61:3528–3546
Liu L, Chen J, Wang Z, Mao ZS, Yang C (2018) Internal mass and heat transfer between a single deformable droplet and simple extensional creeping flow. Int J Heat Mass Transf 127:1040–1053
Liu X, Wang C, Zhao Y, Chen Y (2018) Shear-driven two colliding motions of binary double emulsion droplets. Int J Heat Mass Transf 121:377–389
Liu X, Wang C, Zhao Y, Chen Y (2018) Passing-over motion during binary collision between double emulsion droplets under shear. Chem Eng Sci 183:215–222
Liu HR, Ng CS, Chong KL, Lohse D, Verzicco R (2021) An efficient phase-field method for turbulent multiphase flows. J Comput Phys 446:1–32
Luo ZY, Bai BF (2016) Dynamics of nonspherical compound capsules in simple shear flow. Phys Fluids. https://doi.org/10.1063/1.4965251
Maffettone PL, Minale M (1998) Equation of change for ellipsoidal drops in viscous flow. J Nonnewton Fluid Mech 78:227–241
Magnaudet J, Mercier MJ (2020) Particles, drops, and bubbles moving across sharp interfaces and stratified layers. Annu Rev Fluid Mech 52:61–91
Mandal S, ChakrabortyS, (2017) Effect of uniform electric field on the drop deformation in simple shear flow and emulsion shear rheology. Phys Fluids. https://doi.org/10.1063/1.4995473
Mathai V, Lohse D, Sun C (2020) Bubbly and buoyant particle-laden turbulent flows. Annu Rev Condens Matter Phys 11:529–559
Matsunaga D, Imai Y, Yamaguchi T, Ishikawa T (2015) Rheology of a dense suspension of spherical capsules under simple shear flow. J Fluid Mech 786:110–127
Maxey MR, Riley JJ (1983) Equation of motion for a small rigid sphere in a nonuniform flow. Phys Fluids 26:883–889
Meenu Agrawal KCS, Gaurav A, Karri B (2021) An experimental study of two identical air bubbles rising side-by-side in water. Phys Fluids. https://doi.org/10.1063/5.0044485
Mercier MJ, Wang S, Péméja J, Ern P, Ardekani AM (2019) Settling disks in a linearly stratified fluid. J Fluid Mech. https://doi.org/10.1017/jfm.2019.957
Mohammadi Masiri S, Bayareh M, Ahmadi Nadooshan A (2019) Pairwise interaction of drops in shear-thinning inelastic fluids. Korea Aust Rheol J 31:25–34
Moosaie A, Shekouhi N, Nouri NM, Manhart M (2015) An algebraic closure model for the DNS of turbulent drag reduction by brownian microfiber additives in a channel flow. J Nonnewton Fluid Mech 226:60–66
Moosaie A, Zarghami-Dehaghani Z, Alinejad Z (2017) Rheology of a dilute suspension of brownian thin disklike particles in a turbulent channel flow. J Nonnewton Fluid Mech 286:104414
Nguyen KP, Vu TV (2020) Collision modes of two eccentric compound droplets. Processes. https://doi.org/10.3390/PR8050602
Oldroyd JG (1950) On the formulation of rheological equations of state. Proc Roy Soc London 200:523
Olsson E, Kreiss G (2005) A conservative level set method for two phase flow. J Comput Phys 210:225–246
Pan DY, Lin YQ, Zhang LX, Shao XM (2016) Motion and deformation of immiscible droplet in plane poiseuille flow at low reynolds number. J Hydrodyn 28:702–708
Powell RL (1983) External and internal streamlines and deformation of drops in linear two-dimensional flows. J Colloid Interface Sci 95:148–162
Rosti ME, Brandt L (2018) Suspensions of deformable particles in a couette flow. J Nonnewton Fluid Mech 262:3–11
Santra S, Das S, Chakraborty S (2019) Electric field-induced pinch-off of a compound droplet in poiseuille flow. Phys Fluids. https://doi.org/10.1063/1.5094948
Santra S, Mandal S, Chakraborty S (2019) Confinement effect on electrically induced dynamics of a droplet in shear flow. Phys Rev E 100:33101
Sattari A, Hanafizadeh P, Hoorfar M (2020) Multiphase flow in microfluidics: from droplets and bubbles to the encapsulated structures. Adv Colloid Interface Sci. https://doi.org/10.1016/j.cis.2020.102208
Sattari A, Tasnim N, Hanafizadeh P, Hoorfar M (2021) Motion and deformation of migrating compound droplets in shear-thinning fluids in a microcapillary tube. Phys Fluids 33:53106
Segre S, Silberberg A (1961) Radial particle displacements in poiseuille flow of suspensions. Nature 189:209–210
Shan X, Chen H (1993) Lattice Boltzmann model for simulating flows with multiple phases and components. Phys Rev E 47:1815–1819
Shang X, Luo Z, Bai B (2019) Numerical simulation of dynamic behavior of compound droplets on solid surface in shear flow by front-tracing method. Chem Eng Sci 193:325–335
Shapira M, Haber S (1990) Low reynolds number motion of a droplet in shear flow including wall effects. Int J Multiph flow 16:305–321
Sharaf DM, Premlata AR, Tripathi MK, Karri B, Sahu KC (2017) Shapes and paths of an air bubble rising in quiescent liquids. Phys Fluids 29:1–17
Soligo G, Roccon A, Soldati A (2019) Coalescence of surfactant-laden drops by phase field method. J Comput Phys 376:1292–1311
Soligo G, Roccon A, Soldati A (2020) Deformation of clean and surfactant-laden droplets in shear flow. Meccanica 55:371–386
Starkey TV (1955) The laminar flow of suspensions in tubes. Br J Appl Phys 6:34–37
Sun W, Zhu C, Fu T, Yang H, Ma Y, Li H (2017) The minimum inline coalescence height of bubbles in non-Newtonian fluid. Int J Multiph Flow 92:161–170
Sun W, Zhu C, Fu T, Ma Y, Li H (2019) 3D simulation of interaction and drag coefficient of bubbles continuously rising with equilateral triangle arrangement in shear-thinning fluids. Int J Multiph Flow 110:69–81
Sussman M, Fatemi E (1999) An efficient, interface-preserving level set redistancing algorithm and its application to interfacial incompressible fluid flow. SIAM J Sci Comput 20:1165–1191
Takada N, Tomiyama A, Hosokawa S (2003) Lattice Boltzmann simulation of drops in a shear flow. Fluids Eng Division Summer Meet 36975:495–500

Taylor GI (1932) The viscosity of a fluid containing small drops of another fluid. Proc R Soc London Ser A Contain Pap Math Phys Character 138:41–48
Taylor GI (1934) The formation of emulsions in definable fields of flow. Proc R Soc London Ser A Contain Pap a Math Phys Character 146:501–523
Tiribocchi A, Montessori A, Bonaccorso F, Lauricella M, Succi S (2020) Concentrated phase emulsion with multicore morphology under shear: a numerical study. Phys Rev Fluids 5:1–11
Tripathi MK, Sahu KC, Karapetsas G, Matar OK (2015) Bubble rise dynamics in a viscoplastic material. J Nonnewton Fluid Mech 222:217–226
Tripathi MK, Sahu KC, Govindarajan R (2015) Dynamics of an initially spherical bubble rising in quiescent liquid. Nat Commun 6:1–9
Tryggvason G, Scardovelli R, Zaleski E (2011) Direct numerical simulations of gas–liquid multiphase flows. Cambridge University Press
Uhlmann M (2008) Interface-resolved direct numerical simulation of vertical particulate channel flow in the turbulent regime. Phys Fluids 20:53305
Unverdi SO, Tryggvason G (1992) A front-tracking method for viscous incompressible multi-fluid flows. J comput phys 100(1):25–37
Usefi E, Bayareh M (2020) Numerical simulation of the motion of a Taylor drop in a non-Newtonian fluid. SN Appl Sci 2:42452. https://doi.org/10.1007/s42452-020-2978-7
Van Puyvelde P, Yang H, Mewis J, Moldenaers P (2000) Breakup of filaments in blends during simple shear flow. J Rheol 44:1401–1415
Vladisavljević GT, Al Nuumani R, Nabavi SA (2017) Microfluidic production of multiple emulsions. Micromachines. https://doi.org/10.3390/mi8030075
Vu TV (2019) Parametric study of the collision modes of compound droplets in simple shear flow. Int J Heat Fluid Flow 79:108470
Vu T-V, Vu TV, Bui DT (2019) Numerical study of deformation and breakup of a multi-core compound droplet in simple shear flow. Int J Heat Mass Transf 131:1083–1094
Waele E (1923) Viscometry and plastometry. Oil Color Chem Assoc J 6:33
Wagner AJ (2003) The origin of spurious velocities in lattice Boltzmann. Int J Modern Phys B 17:193–196
Wang W, Li K, Ma M, Jin H, Angeli P, Gong J (2015) Review and perspectives of AFM application on the study of deformable drop/bubble interactions. Adv Colloid Interface Sci 225:88–97
Wang J, Xu S, Huang Y, Guan J (2018) Mechanical mechanisms of the directional shift and inverse of the eccentric compound droplet. Phys Fluids 30:42005
Xu G, Wang X, Xu S, Wang J (2017) Asymmetric rheological behaviors of double-emulsion globules with asymmetric internal structures in modest extensional flows. Eng Anal Bound Elem 82:98–103
Yasuda RAK, Cohen R (1981) Shear-flow properties of concentrated-solutions of linear and star branched polystyrenes. Rheol Acta 20:163
Youngren GK, Acrivos A (1976) On the shape of a gas bubble in a viscous extensional flow. J Fluid Mech 76:433–442
Yue P, Zhou C, Feng JJ, Ollivier-Gooch CF, Hu HH (2006) Phase-field simulations of interfacial dynamics in viscoelastic fluids using finite elements with adaptive meshing. J Comput Phys 219:47–67
Zenit R, Feng JJ (2018) Hydrodynamic interactions among bubbles, drops, and particles in non-newtonian liquids. Annu Rev Fluid Mech 50:505–534
Zhang C, Churazov E, Schekochihin AA (2018) Generation of internal waves by buoyant bubbles in galaxy clusters and heating of intracluster medium. Mon Not R Astron Soc 478:4785–4798
Zhang J, Mercier MJ, Magnaudet J (2019) Core mechanisms of drag enhancement on bodies settling in a stratified fluid. J Fluid Mech 875:622–656
Zhou LX (2009) Two-fluid models for simulating dispersed multiphase flows-a review. J Comput Multiph Flows 1(39–56):2009
Zhu L, Gallaire F (2017) Bifurcation dynamics of a particle-encapsulating droplet in shear flow. Phys Rev Lett 119:1–5
Day P, Manz A, and Zhang Y (2012) Microdroplet technology: principles and emerging applications in biology and chemistry. Springer Science & Business Media.
Elghobashi S (2009) Point-particle model for disperse turbulent flows. Int J Multiph flow 35.
Farhadi J, Sattari A, and Hanafizadeh P (2021) Passage of a rising bubble through a liquid-liquid interface: a flow map for different regimes. Can J Chem Eng.
Fox AJ, Schneider JW, and Khair AS (2021) Dynamics of a sphere in inertial shear flow between parallel walls. J Fluid Mech 915.
JMLeivaEGeffroy2018Evolution of the size distribution of an emulsion under a simple shear flowFluids10.3390/fluids3030046Leiva JM, Geffroy E (2018) Evolution of the size distribution of an emulsion under a simple shear flow. Fluids. https://doi.org/10.3390/fluids3030046
Santra S, Mandal S, and Chakraborty S (2020) Phase-field modeling of multicomponent and multiphase flows in microfluidic systems: a review. Int J Numer Methods Heat Fluid Flow.